



Ultrasensitive Detection of Cancer Cell and Glycan Expression Profiling Based on Multivalent Recognition and Alkaline Phosphatase-Responsive Electrogenerated Chemiluminescence Biosensor

Journal:	<i>Nanoscale</i>
Manuscript ID:	NR-ART-06-2014-003053.R1
Article Type:	Paper
Date Submitted by the Author:	15-Jul-2014
Complete List of Authors:	Chen, Xiaojiao; Tsinghua University, He, Yao; Tsinghua University, Zhang, Youyu; Hunan Normal University, Liu, Meiling; Hunan Normal University, Liu, Yang; Tsinghua university, Department of Chemistry Li, Jinghong; Tsinghua University, Chemistry

Cite this: DOI: 10.1039/c0xx00000x

www.rsc.org/xxxxxx

ARTICLE TYPE

Ultrasensitive Detection of Cancer Cell and Glycan Expression Profiling Based on Multivalent Recognition and Alkaline Phosphatase-Responsive Electrogenerated Chemiluminescence Biosensor

Xiaojiao Chen^{a,b}, Yao He^a, Youyu Zhang^{b,*}, Meiling Liu^b, Yang Liu^{a*} and Jinghong Li^a⁵ Received (in XXX, XXX) Xth XXXXXXXXX 20XX, Accepted Xth XXXXXXXXX 20XX

DOI: 10.1039/b000000x

A multivalent recognition and alkaline phosphatase (ALP)-responsive aptamer electrogenerated chemiluminescence (ECL) biosensor for cancer cell detection and *in situ* evaluating cell surface glycan expression was developed on a poly(amidoamine) (PAMAM) dendrimer conjugated chemically reduced graphene oxide (rGO) electrode interface. In this strategy, the multivalency and high affinity of the cell-targeted aptamers on rGO provided a high efficient cell recognition platform on the electrode. The ALP and concanavalin A (Con A) coated gold nanoparticles (Au NPs) nanoprobe allowed the ALP enzyme-catalyzed production of phenols that inhibited the ECL reaction of Ru(bpy)₃²⁺ on the rGO electrode interface, affording a fast and highly sensitive ECL cytosensing and cell surface glycan evaluation. Combining the multivalent aptamer interface and ALP nanoprobe, an ECL cytosensor showed a detection limit of 38 CCRF-CEM cells mL⁻¹ in human serum samples, broad dynamic range and excellent selectivity. In addition, the proposed biosensor also provided a great insight into dynamically profiling of different glycans expression on cell surface based on the carbohydrate recognized lectins on the nanoprobe, exhibiting a great promising in clinical diagnosis and drug screening.

1. Introduction

Carbohydrate, the key components of cell surface glycolipids and glycoproteins, play critical roles in a wide variety of biological processes including cell growth and differentiation, cell adhesion, cell-cell communication, immune response, pathogen interaction, and intracellular signaling events.¹⁻⁴ The variational expression of cell surface carbohydrate is associated with a variety of diseases, especially neurodegenerative disease and cancers.⁵ Therefore, simultaneous analysis of cell surface carbohydrate expression is essentially important in clinic diagnostic and provides an effective way to monitor the progressions of diseases and understand of their roles in disease development.

Traditional approaches of cell surface glycans analysis including mass spectrometry (MS),⁶⁻⁸ nuclear magnetic resonance (NMR),⁹⁻¹² chromatography^{13, 14} and spectrometry.^{15, 16} Although some of these analysis can provide molecule-level information, they are require complicated sample preparation and unsuitable for dynamically detection due to its destructive nature. Moreover, some methods such as MS and NMR either require valuable equipment or need to be performed by skilled personnel. As an alternative, glyco-biosensors such as lectin arrays^{17, 18} and electrochemical biosensors^{5, 19} by means of the highly specific binding of lectin to carbohydrate have been developed for glycan profiling.⁴ However, the issues of less active-sites accessibility and low affinity between lectin and carbohydrate limit their sensitivity and stability.

Multivalent recognition plays a critical role in a series of binding processes in nature. A multivalency system is proven to enhance the affinity by one to nine orders of magnitude. To realize the maximized multivalency effects for proteins or cells, a majority of biointerfaces have been rationally designed based on

numerous scaffolds.²⁰⁻²² Poly(amidoamine) (PAMAM) dendrimers are the mostly widely used mediator have been reported to be an excellent mediator for facilitated multivalent effect owing to their capability to preorganize/orient ligands and the easy deformability of the polymer chains.^{20, 23} Dramatically increased cell capture efficiency was obtained on an antibody conjugated dendrimer multivalent interface.²³ Recently, the multivalency effects were also observed on nanomaterials scaffolds such as gold nanoparticles, quantum dot for the recognition of carbohydrate, antibody, peptides and DNA.^{20, 24-27} The large accommodation of nanoparticles surface allows more active molecules to be loaded to improve the binding affinity. Moreover, the excellent photonic, electrochemical and mechanical properties of nanoparticles allow them to be excellent transducers with extensive analytical techniques. Graphene, a two-dimensional carbon crystal with only one atom thickness, has drawn much attention because of its excellent electrical conductivity, high surface-to-volume ratio, remarkable chemical stability, easy functionalization and excellent biocompatibility. The unique electric and photo-electrochemical characteristics of graphene have been broadly studied and applied in quantum electrical devices, electromechanical resonators, and electrochemical sensors.²⁸⁻³⁴ Here, PAMAM conjugated graphene (rGO-DEN) composite electrode interface was developed by coupling the unique properties of graphene and PAMAM dendrimer, which can not only improve the electrode interface electron transfer but also enhance the multivalent recognition efficiency, and will be great promising in fabrication of biomimic devices and biosensors with high sensitivity.

Electrogenerated chemiluminescence (ECL) technique combining high controllability inherited from electrochemical modes with low background noise similar to other luminescent

signals, has attracted considerable interest.³⁵ Recently, ECL biosensor is extensively developed for diagnostic purposes, such as aptamer or DNA binding,^{36, 37} enzyme reaction,³⁸ cytosensing.^{39, 40} Tris(2,2'-bipyridyl) ruthenium(II) chloride hexahydrate ($\text{Ru}(\text{bpy})_3^{2+}$) has been the most popular ECL system due to their high efficiency.⁴¹ The $\text{Ru}(\text{bpy})_3^{2+}$ ECL system can be strongly inhibited by many phenol and phenolic analogues based on a "electrochemical oxidation inhibiting" mechanism.^{42, 43} Alkaline phosphatase (ALP) is one of important enzyme that can catalyze the hydrolysis of a group of phosphoryl esters to generate electroactive products.^{44, 45} An ALP catalyzed ECL inhibition system of CdSe nanoparticles has been reported to detect the enzymatic processes in serum samples by the phenolic groups in ALP catalytic products.⁴⁶ The phenol product by ALP catalyzed reaction can also significantly inhibit the $\text{Ru}(\text{bpy})_3^{2+}$ ECL system.^{43, 46} Moreover, the ALP hydrolysis substrate phenyl phosphate disodium (PPNa) has almost no effect on the $\text{Ru}(\text{bpy})_3^{2+}$ ECL signal, showing the great promise in sensitive biosensing applications.⁴⁶

Herein, a multivalent recognition and ALP-responsive aptamer ECL biosensor for cancer cell detection and in situ evaluating cell surface glycan expression was developed on a PAMAM dendrimer conjugated chemically reduced graphene oxide rGO electrode interface (rGO-DEN) (Scheme 1). In this experiment, CCRF-CEM cell (human Acute Lymphoblastic Leukemia) was used as a model cell line, and the abnormal glycan expression on CCRF-CEM cell may be associated with fatal immune deficiency-associated diseases.⁴⁷ An CCRF-CEM cell specific aptamer sgc8c conjugated the rGO-DEN interface were fabricated for highly selective cell capture,⁴⁸ which can not only provide a multivalent recognition interface that dramatically improves the cell capture efficiency but also enhance the electron transfer ability as well as the sensitivity of the biosensor. Besides, lectins and ALP modified gold nanoparticles were prepared as signal probes. Thus, a sandwich type biosensor formed based on the specific interaction between the lectins and the carbohydrates on cell surface. The nanoprobe can inhibit $\text{Ru}(\text{bpy})_3^{2+}$ ECL reaction by the ALP catalytic product phenol in the presence of PPNa, allowing a highly sensitive carbohydrate cancer cell biosensor for human serum samples and open a new way to insight of the physiological functions of glycans in the cellular processes.

2. Experimental sections

Materials and reagents

PPNa, p-Nitrophenyl phosphate disodium salt (PNPP), TPrA and graphite powder (99.99995%, 325mesh) were obtained from Alfa Aesar. Glutaraldehyde (GA) and lectins including Con A, wheat germ agglutinin (WGA) and peanut agglutinin (PNA) were purchased from Sigma-Aldrich. $\text{Ru}(\text{bpy})_3^{2+}$ was purchased from Acros Organics (USA). Bovine serum albumin (BSA) was from Dingguo Biological Products Co. (Beijing, China). $\text{HAuCl}_4 \cdot 3\text{H}_2\text{O}$ (48% w/w) was obtained from Shanghai Reagent (Shanghai, China). The third generation amine-terminated polyamidoamine dendrimers (G3.0 PAMAM-NH₂, abbreviated to be DEN) were purchased from Chenyuan Organosilicon New Material Company (Weihai, China). ALP and aptamer sequences were obtained from Shanghai Sangon Biological Engineering

Technology & Services Co., Ltd. The sequence of sgc8c aptamer is listed as follows: 5'-NH₂-TTT TTT TTT ATC TAA CTG CTG CGC CGC CGG GAA AAT ACT GTA CGG TTA GA- 3'. The use of ALP should with 0.01 M Tris/HCl (pH 8.0) containing 10 mM MgCl₂ and 1 mM ZnCl₂. Tris-HCl buffer (pH 7.4, 10 mM) containing 137 mM NaCl and 2.7 mM KCl was used as washing solution, the Tris buffer (pH 9.0, 50 mM) containing 137 mM NaCl, 2.7 mM KCl, 10 mM MgCl₂ and 1 mM ZnCl₂ was used as detection solution. Human serum was provided by the Affiliated Hospital of Tsinghua University. Other reagents of analytical grade were obtained from Beijing Chemical Company (China) and were used as received.

Apparatus

Transmission electron microscope (TEM) images were collected with a Hitachi H-7650B (Japan) opened at an accelerating voltage of 100 kV. The UV-vis absorption spectra were obtained via a Hitachi U-3900 UV/Vis spectrophotometer (Japan). Fourier transform infrared spectroscopy (FTIR) of samples in KBr pellets was recorded on a Perkin-Elmer Spectrum GX spectrometer (Perkin-Elmer Company, USA). XRD patterns were obtained using a D8 Advance (Bruker) X-ray diffractometer using Cu-K α radiation (1/4 1.5418 Å). Raman spectra were collected on a RM 2000 Microscopic confocal Raman spectrometer (Renishaw PLC, England) with a 633 nm He-Ne laser beam.

The cyclic voltammetry (CV) was conducted on a CHI 440b instrument (CH Instrument Co., USA). Electrochemical impedance spectroscopy (EIS) was carried out on a PARSTAT 2273 potentiostat/galvanostat (Advanced Measurement Technology Inc., USA). Impedance measurements were performed by applying an ac voltage of 5 mV amplitude with frequency from 0.01 Hz to 10⁵ Hz in a 5 mM K₃[Fe(CN)₆]/K₄[Fe(CN)₆] redox probe solution with 0.5 M KCl. The ECL measurements were carried out on an MPI-B multifunctional electrochemical analytical system (Xi'an Remex Analytical Instrument Ltd. Co., China). The voltage of the photomultiplier tube (PMT) was maintained at 600 V.

Synthesis of GO-DEN and rGO-DEN Conjugates

The graphene oxide (GO) was synthesized according to our previous works.^{49, 50} GO-DEN composites were prepared as following. Briefly, 2 mL of DEN solution (50 μM) was added to 2 mL of GO solution (ca. 0.5 mg mL⁻¹) containing KOH (20 mM). The mixture was stirred at 40 °C for 12 h. 160 μL of 0.5 M H₂SO₄ solution was then added and the mixture was further stirred for 30 min. The resulting GO-DEN composites were collected by centrifugation, and washed with DI water for several times. The chemically reduced GO-DEN (rGO-DEN) was obtained by mixing 1 mL of the GO-DEN (ca. 0.3 mg/mL), 15 μL of hydrazine (35 wt% in DI water) and 11.8 μL of ammonia (25 wt% in DI water) at 80 °C for 90 min.

Preparation of ALP-Con A-Au NPs nanoprobe

Au NPs with a diameter of 13 nm were synthesized according to literature procedures.⁵¹ Au NPs were coated with ALP and Con A according to the following method.^{51, 52} Briefly, 1 mL Au NPs

were adjusted to pH 6.2 with 0.1M K_2CO_3 before use. The bioconjugates were freshly prepared by addition of ALP (20 μ L, 1 mg/mL) and Con A (20 μ L, 1 mg/mL) into 1.0 mL of the Au NPs solution. The mixture was then gently stirred at room temperature for 2 h. The excess reagents were removed by centrifugation for 10 min at 10,000 rpm. After discarding the supernatant, the red pellets were washed twice with 10mM Tris buffer (pH 7.4), the resulting ALP-Con A-Au NPs conjugates were finally resuspended in Tris buffer and stored at 4 $^{\circ}C$ for use. The activity of the ALP on the surface of ALP-Con A-Au NPs conjugates was measured by recording the absorbance at 400 nm in the solution the ALP substrate of PNPP.

Cell Culture and Treatments

CCRF-CEM cells were obtained from ATCC (American Type Culture Association). CCRF-CEM cells were cultured in RPMI 1640 medium (Dingguo Biological Products Co., Beijing, China) containing 10% fetal bovine serum (Dingguo), 100 U mL^{-1} penicillin, and 100 U mL^{-1} streptomycin at 37 $^{\circ}C$ in a humidified atmosphere of 5% CO_2 . The cells at the logarithmic growth were collected and separated from the medium by centrifugation at 800 rpm for 5 min and then washed with sterile Dulbecco's phosphate buffer saline (DPBS, pH 7.4) twice. The sediment was then resuspended in DPBS or in human serum to obtain a homogeneous cell suspension. Cell number was determined by using a blood counting chamber.

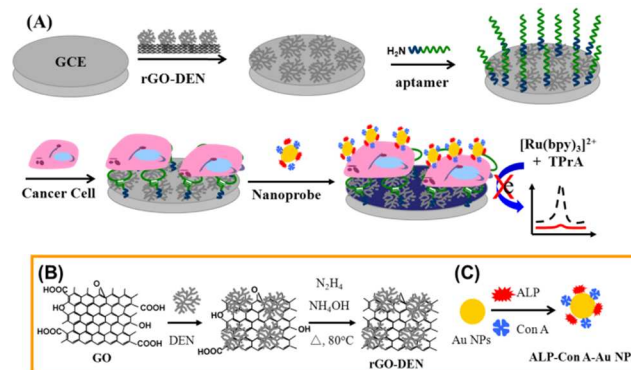
Biosensor Fabrication and Cell Capture

The glassy carbon electrode (GCE, diameter of 3 mm) was polished with 0.3 and 0.05 μ m $\alpha-Al_2O_3$ powder followed by successive sonication in ethanol and distilled water respectively. After being dried with high-purity nitrogen gas, 6 μ L of 1mg mL^{-1} rGO-DEN solution was dropped onto GCE and dried overnight to fabricate a functional film (rGO-DEN/GCE). Subsequently, the electrode was immersed in 100 μ L of 2.5% GA solution for 1 h to activate amine group on the film surface. Then, 50 μ L of 1 μ M sgc8c aptamer solution was added to the film and incubated for 1 h (aptamer/rGO-DEN/GCE). The electrode surface was then rinsed with washing buffer and dried in a nitrogen gas stream. Whereafter, 200 μ L sample prepared by dispersing a certain amount of CCRF-CEM cells in DPBS was added on the sgc8c modified surface and incubated at 37 $^{\circ}C$ for 1.5 h. Following a rinse with buffer, CCRF-CEM cell/aptamer/rGO-DEN/GCE electrode was obtained.

ECL measurements of ALP-Con A-Au NPs Nanoprobe-Based Cell Surface N-Glycan Expression

The CCRF-CEM cell/aptamer/rGO-DEN/GCE electrode was incubated with 30 μ L of ALP-Con A-Au NPs nanoprobe solution containing 1 mM Ca^{2+} and Mn^{2+} for 1 h. The nanoprobe was captured via the specific binding between Con A and cell surface mannose and trimannoside. Here, the Ca^{2+} and Mn^{2+} were necessary for the activity of Con A binding to cell surface mannose. After carefully rinsed with PBS, the prepared ALP-Con A-Au NPs/CCRF-CEM cell/aptamer/rGO-DEN/GCE electrode was immersed in 2 mL Tris-HCl (pH 9.0, 50 mM) solution with 0.25 mM TPrA, 75 μ M $(Ru(bpy)_3)^{2+}$ and 4 mM PPNa for 20 min.

The ECL measurements were performed from 0 to 1.25 V with scan rate of 100 $mV s^{-1}$ using Ag/AgCl electrode with saturated KCl solution and platinum wire as the reference electrode and counter electrode, respectively.



Scheme 1 (A) Schematic illustration of the aptamer ECL biosensor sensor based on the multivalent recognition and ALP responsive signal amplification for sensitive cell detection and cell surface carbohydrate evaluation. (B) Synthesis of rGO-dendrimer conjugates. (C) Fabrication procedures of ALP-Con A-AuNPs nanoprobe.

3. Results and discussion

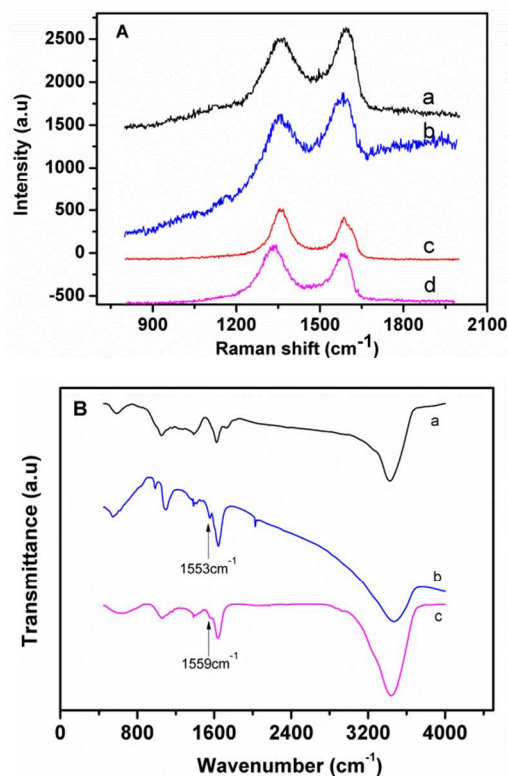


Fig.1 The Raman spectra (A) of GO (a), GO/DEN (b), rGO (c) and rGO/DEN (d), and FTIR spectra (B) of GO (a), Dendrimer (b) and rGO/DEN (c).

Scheme 1 presents the ECL biosensor for cytosensing and cell surface carbohydrate evaluation based on multivalent recognition and dual signal amplification. The PAMAM dendrimer conjugated rGO was firstly fabricated and modified onto the GCE, which can not only promote the interface electron transfer

rate but also afford a large accommodation for aptamer conjugation. The dendrimer mediated multivalent binding between aptamer and cancer cells could improve the cell capture efficiency and thus enhance the sensitivity of the biosensor. The cell captured electrode was then incubated with the ALP-Con A-Au NPs nanoprobe to form a sandwich type system based on the specific recognition between the lectin and carbohydrate on cell surface, obtaining high selectivity and sensitivity for cell detection as well as the surface glycan analysis. Meanwhile, ALP-Con A-Au NPs exploit the amplification effect of Au NPs for loading a large number of lectins and ALP, and significantly inhibit Ru(bpy)₃²⁺ ECL signal.⁵³ Therefore, the sensitivity of the biosensor is greatly enhanced.

Fig. 1A shows the Raman spectra of the forming of rGO-DEN composites. The characteristic spectrum of GO or rGO are focused at two main bands, the G mode (usually observed at ~1580 cm⁻¹) and the D mode (at ~1350 cm⁻¹).⁵⁴ The relative intensity of the D and G bands (D/G) reflects the electronic conjugation state of graphene derivate. When GO was reduced, the intensity ratio of D mode and D mode increases, indicating the formation of rGO. It's clear that rGO-DEN keeps the original properties of rGO in the process of assembling GO with PAMAM and reduction with hydrazine hydrate.

FTIR was also used to confirm the conjugation of rGO-DEN. In Fig. 1B, the peaks of GO (curve a) at 1624 and 1729 cm⁻¹ correspond to the stretching vibrations of C=C and C=O respectively, which demonstrate the carboxylic group existing on the surface of GO. The pure PAMAM give absorption bands at 1646 and 1553 cm⁻¹, assigned to C=O stretching (amide I) and N-H bending/C-N stretching (amide II) vibrations of the dendrimer interior, respectively (curve b).⁵⁵ After PAMAM coupling and hydrazine reducing, absorption bands at 1638 and 1559 cm⁻¹ were observed, and the characteristic absorption peaks of carboxylic group at 1729 cm⁻¹ was disappeared, indicating the formation of PAMAM conjugated rGO composite which also kept the well-defined nanosheet structure (Fig. S1C).

Au NPs with a diameter of about 20 nm were used and conjugated with Con A and ALP. The Au NPs were characterized by UV-vis spectrometry and TEM (Fig. S1A in Supporting Information). After the conjugation of Con A and ALP, the characteristic absorption peak of gold nanoparticles red shift from 522 nm to 528 nm due to the decoration of biomolecules on Au nanoparticles. The activity of the ALP-Con A-Au NPs nanoprobe was verified by UV-Vis. (Fig. S1B). In the presence of ALP, the colourless PNPP was catalyzed to produce p-nitrophenol (PNP), a bright yellow product (insert in Fig. S1B). Accordingly, the absorption peak at 310 nm of the solution was decreased, and a distinct absorption peak at 400 nm was observed (curve c). The result demonstrated that ALP-Con A-Au NPs nanoprobe has excellent activity.

Cyclic voltammetry (CV) and electrochemical impedance spectroscopy (EIS) are used to verify the stepwise assembly of the cytosensor.³⁹ Both the bare GCE (curve a) and rGO-DEN modified GCE (curve b) exhibited a couple of reversible redox peaks as shown in Fig. S2A (Supporting Information), and an increasing current intensity presented on the rGO-DEN/GCE, ascribing to the large surface and the excellent conductivity of rGO-DEN composite. After immersing into sgc8c aptamer, the

current decreased (curve c) due to the electron inert feature of the aptamer. The peak currents were further decreased, and the gap between the anodic and cathodic peaks became wider after subsequent capture of CCRF-CEM cells by the specific recognizing of sgc8c to the cell surface PTK7 (curve d). Moreover, the electron transfer between the redox probe and electrode was further hindered after incubation with ALP-Con A-Au NPs probes because of the electrostatic repulsion between negatively charged Con A and citrate anions on Au NPs and Fe(CN)₆^{4-/3-} (curve e). Fig. S2B shows the Nyquist plots of EIS upon the stepwise modification processes. Nyquist plots composed of a semicircle portion at higher frequencies corresponding to the electron-transfer-limited process and a linear portion at lower frequencies representing the diffusion limited process. The semicircle diameter equals to the electron transfer resistance (R_{et}). Due to the good conductivity of rGO, the rGO-DEN/GCE (curve b) displayed a lower resistance than bare GCE (curve a). Afterwards, the R_{et} increased successively with sequential assembly of sgc8c aptamer (curve c), capture of CCRF-CEM cell (curve d), and incubation of nanoprobe (curve e), which was well consistent with that of CV and demonstrated the feasibility of the biosensor.

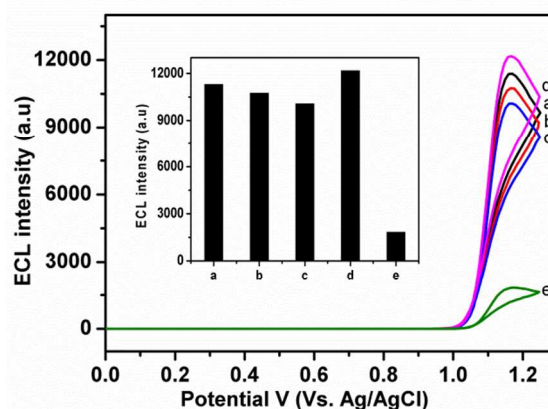


Fig. 2 ECL intensity-potential curves of aptamer/rGO-DEN/GCE (a), cell/aptamer/rGO-DEN/GCE (b), ALP-Con A-Au NPs/aptamer/rGO-DEN/GCE (c), ALP-Con A-Au NPs/cell/rGO-DEN/GCE (d), and ALP-Con A-Au NPs/CCRF-CEM cell/aptamer/rGO-DEN/GCE (e) in 50 mM Tris/HCl (pH 9.0) containing 0.25 mM TPA, 75 uM Ru(bpy)₃²⁺ and 4mM PPNa. Scan rate, 100 mV/s. The PMT voltage is 600 V. The concentration of CCRF-CEM cells: 1.0×10^5 cells mL⁻¹. Inset: Values of the peak intensities of the corresponding ECL curves at 1.25V.

Fig. 2 shows the ECL behaviours of the biosensor in 50 mM Tris buffer (pH 9.0) containing 0.25 mM TPA, 75 uM Ru(bpy)₃²⁺ and 4mM PPNa. The aptamer/rGO-DEN/GCE exhibited a strong ECL emission of Ru(bpy)₃²⁺ starts at about 1.0 V with a peak at around 1.15 V in the presence of TPA (curve a). The ECL intensity decreased after immersing the aptamer/rGO-DEN/GCE electrode in the cell solution due to the multivalent recognition between the sgc8c aptamer conjugated rGO-DEN interface and PTK7 on the CCRF-CEM cell surface (curve e). The high ECL signal was attributed to the reaction between Ru(bpy)₃²⁺ and TPA. When the cell adsorbed electrode was treated with the ALP-Con A-Au NPs, a sharp decrease of the ECL signal was observed, attributing to the phenolic groups of ALP catalytic products that significantly inhibited Ru(bpy)₃²⁺ ECL reaction. To verify the ECL signals come from the multivalent recognition

between the aptamers and cell as well as the specific binding between the nanoprobe and cells, the aptamer/rGO-DEN/GCE was incubated in the solution with CCRF-CEM cells (curve b) or ALP-Con A-Au NPs nanoprobe separately (curve c). It was clear that both of the electrode presented high responses which was closed to the background. The reason is that the aptamer modified electrode can be built to the intact ALP-responsive $\text{Ru}(\text{bpy})_3^{2+}$ -

TPrA ECL inhibition system only in the presence of both cell or nanoprobe. In addition, the rGO-DEN/GCE did not immobilize sgc8c aptamer followed by incubating with cell and nanoprobe also exhibited an intensive response (curve d), which suggested that sgc8c aptamer modified electrode can selectively recognize and capture the CCRF-CEM cell surface, and the nonspecific adsorption was very weak.

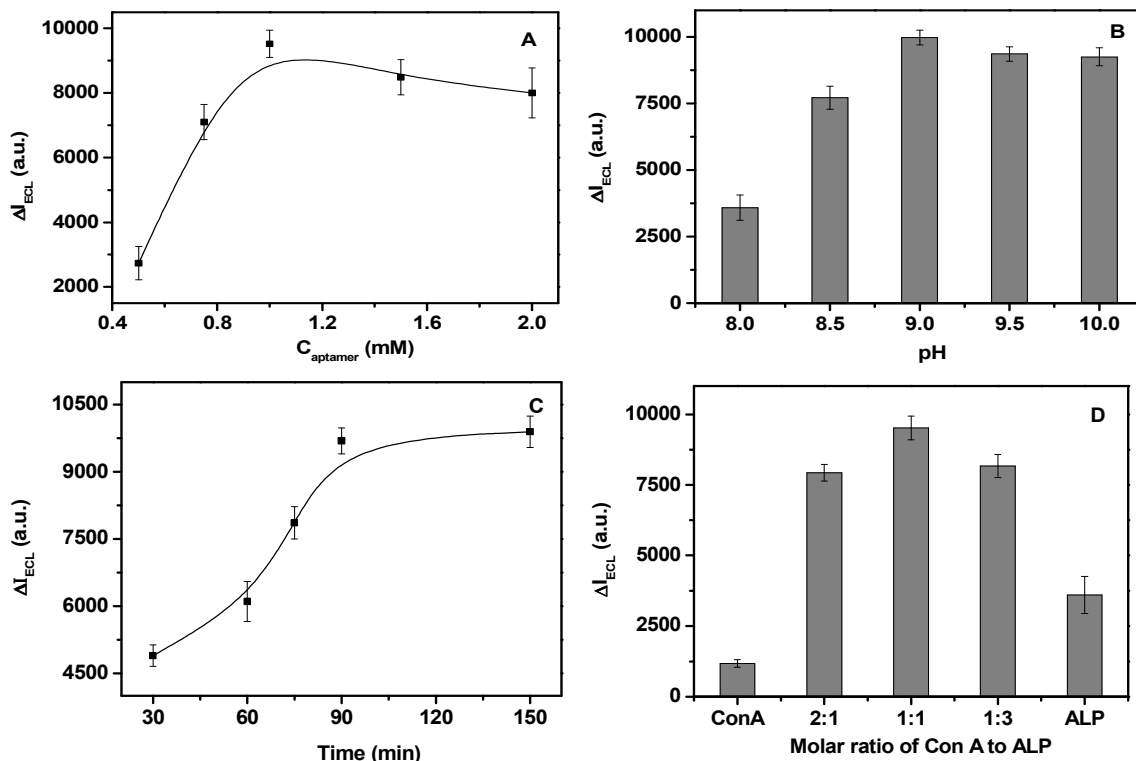


Fig. 3 Optimization of (A) aptamer concentration, (B) pH value, (C) cell incubation time and (D) molar ratio of ALP to Con A used for preparation of nanoprobe in 50 mM Tris (pH9.0) containing 0.25 mM TPA, 75 μM $\text{Ru}(\text{bpy})_3^{2+}$ and 4 mM PPNa. Error bars represent standard deviations from three independent experiments. CV Scan rate, 100 mV/s. The PMT voltage is 600 V. The concentration of CCRF-CEM cell is 1.0×10^5 cells mL^{-1} .

The numbers of the aptamer on the electrode plays an important role on the cell capture and the sensitivity of the biosensor. As a result, the aptamer conjugated electrodes were fabricated by dropping the rGO-DEN/GCE in the solution with different concentrations of aptamer. As shown in Fig. 3A, the ECL intensity change increased with the aptamer concentration from 0.5 to 1.0 mM, demonstrating that more CCRF-CEM cells were captured. After that, the ECL intensity change decrease which could be ascribed to the steric hindrance of the large numbers of aptamer and cells on the electrode interface. Therefore, the concentration of 1.0 mM of the aptamer precursor solution was used. The pH effect on the biosensor performances was also studied. The ECL signal changes in 50 mM Tris-HCl buffer with pH values varying from 8.0 to 10.0 were recorded (Fig. 3B). The change of ECL response increased as the pH increased from 8.0 to 9.0 and then decreased at pH higher than 9.0. The weak ECK response at lower pH was attributed to the low activity of ALP in hydrolysis, and the decrease of response at high pH might cause by desorption of the cell in strong alkalis condition. Thus, all subsequent experiments were performed in 50 mM Tris-HCl buffer with a pH of 9.0. Furthermore, the binding time between aptamer and cells was also a crucial factor

on the cell capture. It was observed that the ECL intensity changes elevated with increasing incubation time and reached an approximate plateau at 90 min (Fig. 3C). Thereby, 90 min was applied as the best recognition time. In addition, the effect of molar ratio of ALP to Con A used for preparation of nanoprobe was also discussed. At a constant total protein weight, the ECL response changes increased with the increasing molar ratio of ALP to Con A until 1:1, followed by a sharp decrease, which was due to the fact that the recognition protein on the nanoprobe was insufficient for binding to CCRF-CEM cells. As a result, 1:1 of the ratio of ALP to Con A was used for the preparation of the nanoprobe.

The highly sensitive and selective detection of cancer cells from human serum plays an important role in early cancer diagnosis, and thus greatly increases the chance for effective treatment.⁵⁶ Under the optimized conditions, we investigated the performance of the developed aptamer sensor in quantitative analysis of cancer cells. Fig. 4A presents the ECL signals of the biosensor responding to CCRF-CEM cells. Upon increasing the concentration of CCRF-CEM cell, the ECL intensity decreased due to the ECL inhibition of ALP hydrolysate phenol. The ECL intensity changes between the ECL signal without cells and with

cells at different concentrations was recorded. The inset of Fig. 4A displays the relationship between the ECL intensity changes (ΔI_{ECL}) as a function of the logarithmic value of the concentration of CCRF-CEM cells. A good linear relationship was obtained in the range of 1.0×10^2 to 1.0×10^5 cells mL^{-1} . The linear regression equation is ΔI_{ECL} (au) = $2532.8 \times \log C_{cell}$ (cells mL^{-1}) - 3066.0 with a correlation coefficient of 0.9950 ($n=3$), where ΔI_{ECL} is the ECL signal changes and C_{cell} is the CCRF-CEM cell concentrations. The detection limit is estimated to be 38 cells mL^{-1} at 3σ . It is obvious that the sensitivity of multivalent recognition and dual signal amplification strategy is much higher than those cytosensors using Con A as the capture or recognition element reported in the literatures.^{30, 57-59} It is reasonable that the ECL cytosensor is based on the covalent attachment of aptamer to the rGO-DEN. The large number of aptamers mediated by PAMAM affords a multivalent binding effect that significantly enhances the cancer cell capture efficiency. In addition, compared to the weak affinity between lectin and carbohydrate, the high affinity between the aptamer and cells also intensively improves both of the binding efficiency and selectivity of the cells on the electrode interface, and enhances both of the sensitivity and selectivity of the biosensor.

The determination of different cell lines such as CCRF-CEM (human Acute Lymphoblastic Leukemia, a), Ramos (Human Burkitt's lymphoma cell line, b), K562 (human immortalised myelogenous leukemia, c), MCF-7 (human breast adenocarcinoma cell line, d), A549 (human alveolar basal epithelial cells, e) and BEAS-2B (human bronchial epithelial cell, f) cell line were studied as shown in Fig. 4B. A significantly ECL response was obtained for the CCRF-CEM cells, whereas a small response is observed for the other cell lines even though the Ramos and K562 cell also belong to leukemia cell line. This result demonstrates the excellent selectivity of the proposed sensor, which is promising in the applications of circled tumor cell detection and histopathological lesion studies.

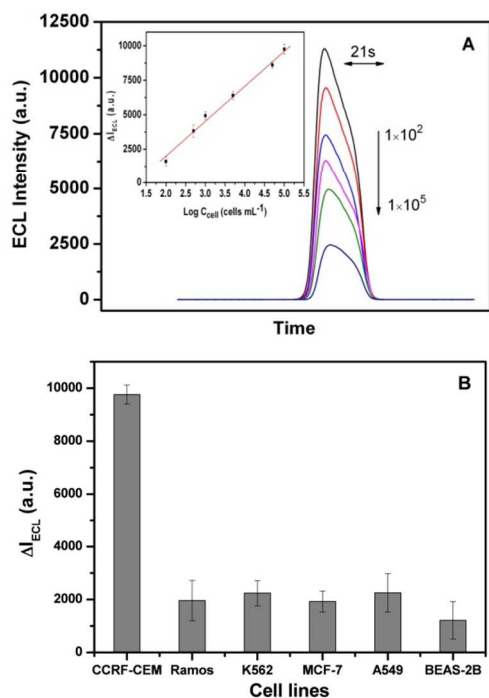


Fig. 4 (A) ECL intensity-time curves of the aptasensor after incubation with CCRF-CEM cell at different concentrations (from 0, 1.0×10^2 , 5.0×10^2 , 1.0×10^3 , 5.0×10^3 , 5.0×10^4 , to 1.0×10^5 cells mL^{-1} respectively) in 50 mM Tris/HCl (pH 9.0) containing 0.25 mM TPA, 75 μM $\text{Ru}(\text{bpy})_3^{2+}$ and 4 mM PPNa. Inserts are the plots of ECL intensity changes vs logarithm of CCRF-CEM cell concentration. Error bars represent standard deviations from three independent experiments. (B) The ECL changes of the biosensor treated with various cancer cell lines. All measurements were performed with as cell concentration of 1.0×10^5 cells mL^{-1} . Scan rate, 100 mV/s. The PMT voltage, 600 V.

To further demonstrate the feasibility of the developed biosensor, the detection of CCRF-CEM cancer cells in human serum were carried out. A gradual decrease in the ECL intensities was observed with increasing CCRF-CEM cell in human serum in the range from 10^2 to 10^5 cells. The ECL intensity changes and the logarithm of cell concentration also represent a linear relationship like that in PBS solution. The sensitivity of the ECL biosensor for human serum samples was almost the same as that in PBS, revealing that the developed biosensor can be used for circled tumor cell detection from peripheral blood.

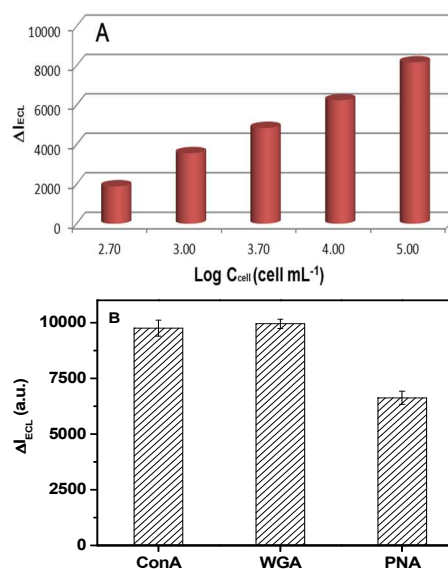


Fig. 5 (A) ECL intensity-time curves of ALP-Con A-Au NPs/CCRF-CEM cell/aptamer/rGO-DEN modified GCE in response to CCRF-CEM cell in 200 μL human serum (from a to f: 0, 5.0×10^2 , 1.0×10^3 , 5.0×10^3 , 1.0×10^4 , and 1.0×10^5 cells mL^{-1} respectively). (B) The ECL changes of different lectin - recognized glycans on ALP-lectin-AuNPs/CCRF-CEM cell/aptamer/rGO-DEN modified GCE. ECL intensity was recorded in 50 mM Tris/HCl (pH 9.0) containing 0.25 mM TPA, 75 μM $\text{Ru}(\text{bpy})_3^{2+}$ and 4 mM PPNa. CV Scan rate, 100 mV/s. The PMT voltage: 600 V. Potential: 0-1.25 V (vs Ag/AgCl). The error bars represent RSD across three repetitive experiments.

The high sensitivity of the ECL biosensor allows it to be used for dynamic cell surface carbohydrate expression evaluation. To analysis the different cell surface carbohydrates expression, nanoprobe with different lectins, such as Con A, PNA, and WGA, were prepared respectively. The ALP-lectin-Au NPs nanoprobe with distinct binding specificities (table S1) was used to evaluate the carbohydrate expression on CCRF-CEM cell surface. Under the similar condition, the different carbohydrate expressions on CCRF-CEM cell surface were monitored. Fig. 5B shows the ECL intensity changes by using the nanoprobe with various lectins that reflecting the coordinative carbohydrates

expression levels of distinct membrane glycan motifs. The results indicate that high level of Con A and WGA-specific glycans are expressed on the CCRF-CEM cell surface. As a comparison, the PNA-specific glycans expression level is low. As for the important role of cell surface carbohydrate on a series of biological processes such as cell growth and differentiation, cell adhesion as well as the associated diseases such as cancer etc., the ECL biosensor provide a promising platform on the studies of carbohydrate related disease as well as drug screening.

4. Conclusion

An ultrasensitive cytosensor for in situ evaluating cell surface carbohydrate expression has been developed by combining the signal amplification of ALP-Con A-Au NPs nanoprobe, the specific binding of sgc8c aptamer and Con A, with ALP-responsive ECL inhibition methods. Based on the multivalent aptamer interface and ALP nanoprobe, the ECL cytosensor showed a detection limit of 38 cells mL⁻¹ in human serum samples, broad dynamic range and excellent selectivity. In addition, the proposed biosensor also provided a great insight into dynamically profiling of carbohydrate expression on cell surface based on the carbohydrate recognized lectins on the nanoprobe, exhibiting a great promising in clinical diagnosis and drug screening. Given the crucial roles of carbohydrate in a series of biological processes and diseases, the sensitive and universal ECL sensing platform is promising in developing on-chip, high-throughput assays for glycomics studies as well as clinical diagnostics and drug screening.

5. Acknowledgements

This work was financially supported by the National Natural Science Foundation of China (No. 21375073, No. 21005046, No. 21235004, No. 21275051) and National Basic Research Program of China (No. 2011CB935704, No. 2013CB934004).

Notes and references

^aDepartment of Chemistry, Beijing Key Laboratory for Analytical Methods and Instrumentation, Tsinghua University, Beijing 100084, China.

^bKey Laboratory of Chemical Biology and Traditional Chinese Medicine Research (Ministry of Education), College of Chemistry and Chemical Engineering, Hunan Normal University, Changsha 410081, China

Phone: +86-10-62795290. Fax: +86-10-62771149. E-mail:

liu-yang@mail.tsinghua.edu.cn; zhangyy@hunnu.edu.cn

† Electronic supplementary information (ESI) available: CV and EIS during the electrode assembly, activity of the nanoprobe and the glycan-binding specificities of the lectins. See DOI: 10.1039/b000000x/

1. R. J. Linhardt and T. Toshihiko, *Acc. Chem. Res.*, 2004, **37**, 431-438.
2. J. Balzarini, *Nat. Rev. Microbiol.*, 2007, **5**, 583-597.
3. J. Hirabayashi, *J. Biochem.*, 2008, **144**, 139-147.
4. S. Cunningham, J. Q. Gerlach, M. Kane and L. Joshi, *Analyst*, 2010, **135**, 2471-2480.
5. X. A. Zhang, Y. Q. Teng, Y. Fu, L. L. Xu, S. P. Zhang, B. He, C. G. Wang and W. Zhang, *Anal. Chem.*, 2010, **82**, 9455-9460.
6. X. Liu, D. J. McNally, H. Nothhaft, C. M. Szymanski, J. R. Brisson and J. J. Li, *Anal. Chem.*, 2006, **78**, 6081-6087.

7. K. Kaneshiro, M. Watanabe, K. Terasawa, H. Uchimura, Y. Fukuyama, S. Iwamoto, T. A. Sato, K. Shimizu, G. Tsujimoto and K. Tanaka, *Anal. Chem.*, 2012, **84**, 7146-7151.
8. T. Nishikaze, K. Kaneshiro, S. Kawabata and K. Tanaka, *Anal. Chem.*, 2012, **84**, 9453-9461.
9. W. A. Bubb, *Concept Magn. Reson. A*, 2003, **19A**, 1-19.
10. C. T. Weller, J. Lustbader, K. Seshadri, J. M. Brown, C. A. Chadwick, C. E. Kolthoff, S. Ramnarain, S. Pollak, R. Canfield and S. W. Homans, *Biochemistry*, 1996, **35**, 8815-8823.
11. A. W. Barb, L. Meng, Z. Gao, R. W. Johnson, K. W. Moremen and J. H. Prestegard, *Biochemistry*, 2012, **51**, 4618-4626.
12. X. Song, Y. Lasanajak, B. Xia, D. F. Smith and R. D. Cummings, *ACS Chem. Biol.*, 2009, **4**, 741-750.
13. S. Park, J. W. Sung and I. Shin, *ACS Chem. Biol.*, 2009, **4**, 699-701.
14. M. A. Bynum, H. Yin, K. Felts, Y. M. Lee, C. R. Monell and K. Killeen, *Anal. Chem.*, 2009, **81**, 8818-8825.
15. S. H. Lim, C. J. Musto, E. Park, W. Zhong and K. S. Suslick, *Org. Lett.*, 2008, **10**, 4405-4408.
16. T. W. Powers, E. E. Jones, L. R. Betesh, P. R. Romano, P. Gao, J. A. Copland, A. S. Mehta and R. R. Drake, *Anal. Chem.*, 2013, **85**, 9799-9806.
17. S. Park, W. Kim, Y. Kim, Y. D. Son, S. C. Lee, E. Kim, S. H. Kim, J. H. Kim and H. S. Kim, *Anal. Chem.*, 2010, **82**, 5830-5837.
18. I. Shin, S. Park and M.-r. Lee, *Chem. Eur. J.*, 2005, **11**, 2894-2901.
19. W. Cheng, L. Ding, S. Ding, Y. Yin and H. Ju, *Angew. Chem. Int. Ed.*, 2009, **48**, 6465-6468.
20. L. Gu, P. G. Luo, H. Wang, M. J. Mezziani, Y. Lin, L. M. Veca, L. Cao, F. Lu, X. Wang, R. A. Quinn, W. Wang, P. Zhang, S. Lacher and Y.-P. Sun, *Biomacromolecules*, 2008, **9**, 2408-2418.
21. R. V. Vico, J. Voskuhl and B. J. Ravoo, *Langmuir*, 2010, **27**, 1391-1397.
22. S. Ikeda, Y. Mori, Y. Furuhashi and H. Masuda, *Solid State Ionics*, 1999, **121**, 329-333.
23. J. H. Myung, K. A. Gajjar, J. Saric, D. T. Eddington and S. Hong, *Angew. Chem. Inter. Ed.*, 2011, **50**, 11769-11772.
24. Y. Z. Wang, Z. H. Chen, Y. Liu and J. H. Li, *Nanoscale*, 2013, **5**, 7349-7355.
25. J. M. de la Fuente and S. Penadés, *Tetrahedron: Asymmetry*, 2005, **16**, 387-391.
26. C. Earhart, N. R. Jana, N. Erathodiyil and J. Y. Ying, *Langmuir*, 2008, **24**, 6215-6219.
27. J. M. de la Fuente, A. G. Barrientos, T. C. Rojas, J. Rojo, J. Cañada, A. Fernández and S. Penadés, *Angew. Chem. Inter. Ed.*, 2001, **40**, 2257-2261.
28. A. D. Elbein, *Annu. Rev. Biochem.*, 1987, **56**, 497-534.
29. L. H. Tang, Y. Wang, Y. M. Li, H. B. Feng, J. Lu and J. H. Li, *Adv. Funct. Mater.*, 2009, **19**, 2782-2789.
30. J. Deng, M. Liu, F. Lin, Y. Zhang, Y. Liu and S. Yao, *Anal. Chim. Acta*, 2013, **767**, 59-65.
31. Z. Wang, J. Zhang, P. Chen, X. Zhou, Y. Yang, S. Wu, L. Niu, Y. Han, L. Wang, F. Boey, Q. Zhang, B. Liedberg and H. Zhang, *Biosens. Bioelectron.*, 2011, **26**, 3881-3886.
32. Z. Yin, Q. He, X. Huang, J. Zhang, S. Wu, P. Chen, G. Lu, Q. Zhang, Q. Yan and H. Zhang, *Nanoscale*, 2012, **4**, 293-297.
33. Z. Wang, S. Wu, J. Zhang, P. Chen, G. Yang, X. Zhou, Q. Zhang, Q. Yan and H. Zhang, *Nanoscale Res. Lett.*, 2012, **7**, 161.

-
34. X. Huang, Z. Yin, S. Wu, X. Qi, Q. He, Q. Zhang, Q. Yan, F. Boey and H. Zhang, *Small*, 2011, **7**, 1876-1902.
35. W. Miao, *Chem. Rev.*, 2008, **108**, 2506-2553.
36. L. Hu, Z. Bian, H. Li, S. Han, Y. Yuan, L. Gao and G. B. Xu, *Anal. Chem.*, 2009, **81**, 9807-9811.
37. R. Gill, R. Polsky and I. Willner, *Small*, 2006, **2**, 1037-1041.
38. S. Xu, Y. Liu, T. Wang and J. Li, *Anal. Chem.*, 2011, **83**, 3817-3823.
39. Y. Z. Wang, Z. H. Chen, Y. Liu and J. H. Li, *Nanoscale*, 2013, **5**, 7349-7355.
40. Z. Chen, Y. Liu, Y. Wang, X. Zhao and J. Li, *Anal. Chem.*, 2013, **85**, 4431-4438.
41. G. A. Crespo, G. Mistlberger and E. Bakker, *Chem. Commun.*, 2011, **47**, 11644-11646.
42. J. McCall, C. Alexander and M. M. Richter, *Anal. Chem.*, 1999, **71**, 2523-2527.
43. Y. Chi, Y. Dong and G. N. Chen, *Anal. Chem.*, 2007, **79**, 4521-4528.
44. M. R. Akanda, M. A. Aziz, K. Jo, V. Tamilavan, M. H. Hyun, S. Kim and H. Yang, *Anal. Chem.*, 2011, **83**, 3926-3933.
45. M. R. Akanda, V. Tamilavan, S. Park, K. Jo, M. H. Hyun and H. Yang, *Anal. Chem.*, 2013, **85**, 1631-1636.
46. H. Jiang and X. Wang, *Anal. Chem.*, 2012, **84**, 6986-6993.
47. M. Matsuoka and K. T. Jeang, *Oncogene*, 2011, **30**, 1379-1389.
48. Y. Chen, M. B. O'Donoghue, Y. F. Huang, H. Kang, J. A. Phillips, X. Chen, M. c. Estevez, C. J. Yang and W. Tan, *J. Am. Chem. Soc.*, 2010, **132**, 16559-16570.
49. J. M. Kim and J. Kim, *Chem. Commun.*, 2012, **48**, 9233-9235.
50. M. A. Herrero, J. Guerra, V. S. Myers, M. V. Gomez, R. M. Crooks and M. Prato, *ACS Nano*, **4**, 905-912.
51. J. Liu and Y. Lu, *Nat. Protoc.*, 2006, **1**, 246-252.
52. W. W. Zhao, Z. Y. Ma, D. Y. Yan, J. J. Xu and H. Y. Chen, *Anal. Chem.*, 2012, **84**, 10518-10521.
53. Y. Liu, Y. Liu, H. Feng, Y. Wu, L. Joshi, X. Zeng and J. Li, *Biosens. Bioelectron.*, 2012, **35**, 63-68.
54. Z. Luo, L. Yuwen, Y. Han, J. Tian, X. Zhu, L. Weng and L. Wang, *Biosens. Bioelectron.*, 2012, **36**, 179-185.
55. A. Manna, T. Imae, K. Aoi, M. Okada and T. Yogo, *Chem. Mater.*, 2001, **13**, 1674-1681.
56. H. Liu, S. Xu, Z. He, A. Deng and J.-J. Zhu, *Anal. Chem.*, 2013, **85**, 3385-3392.
57. Z. Qian, H.-J. Bai, G.-L. Wang, J.-J. Xu and H.-Y. Chen, *Biosens. Bioelectron.*, 2010, **25**, 2045-2050.
58. E. Han, L. Ding, S. Jin and H. Ju, *Biosens. Bioelectron.*, 2011, **26**, 2500-2505.
59. Z. Chen, Y. Liu, Y. Wang, X. Zhao and J. Li, *Anal. Chem.*, 2013, **85**, 4431-4438.

Scheme 1

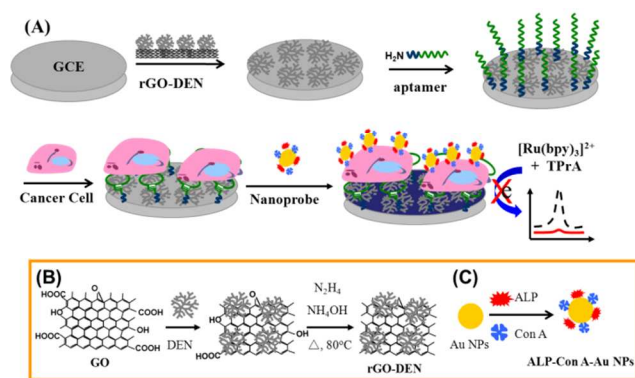


Fig. 1

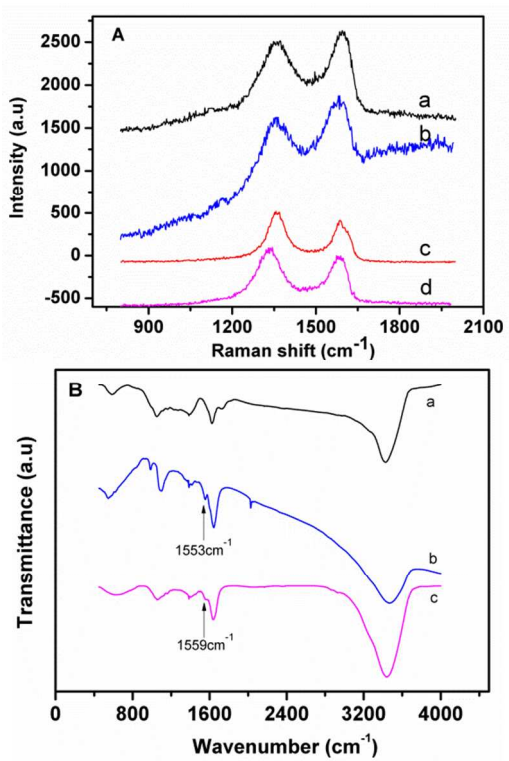
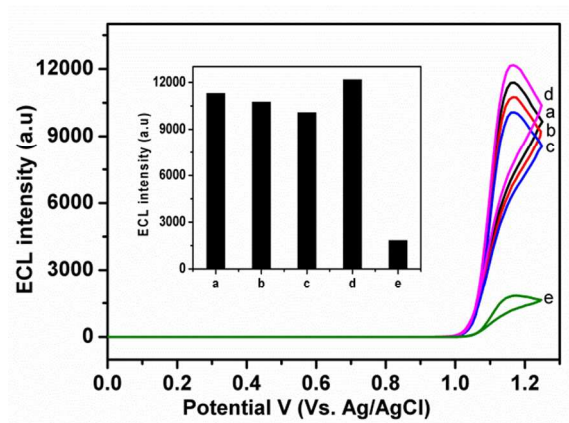


Fig. 2



Cite this: DOI: 10.1039/c0xx00000x

www.rsc.org/xxxxxx

ARTICLE TYPE

Fig. 3

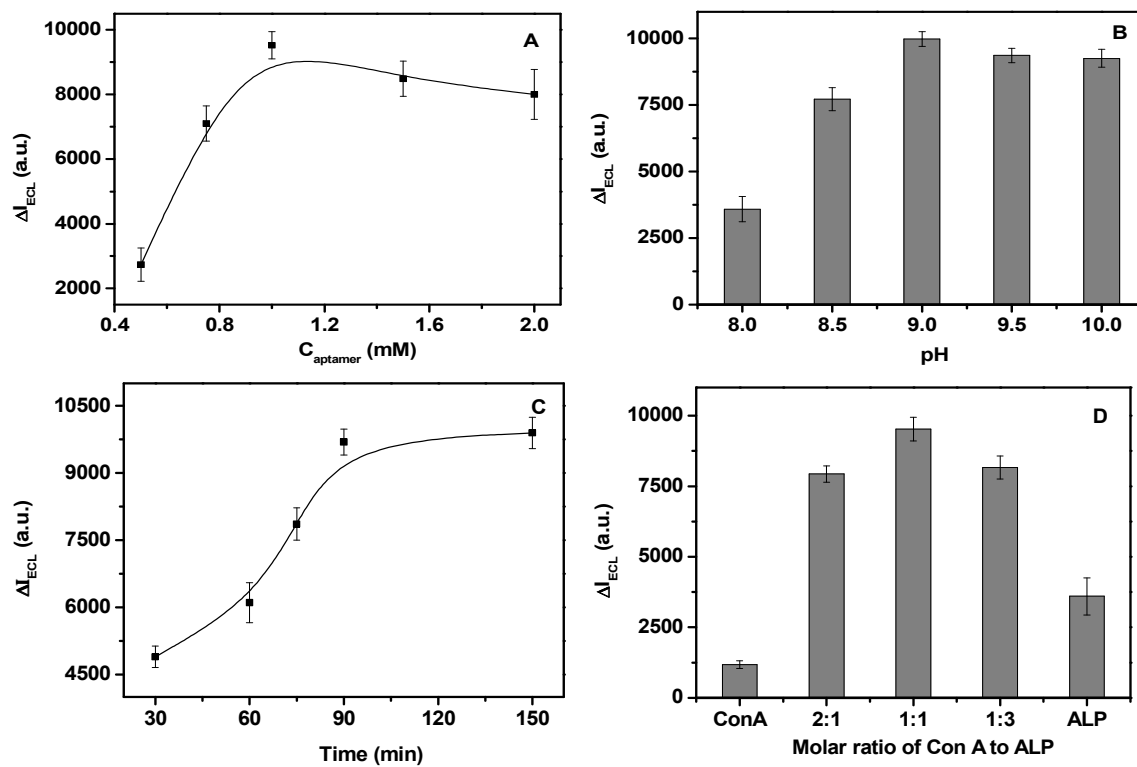


Fig./Scheme XX Caption

5

Fig. 4

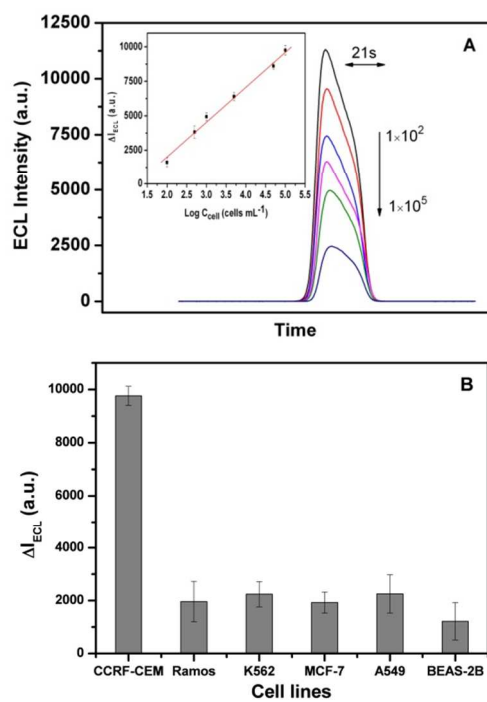


Fig. 5

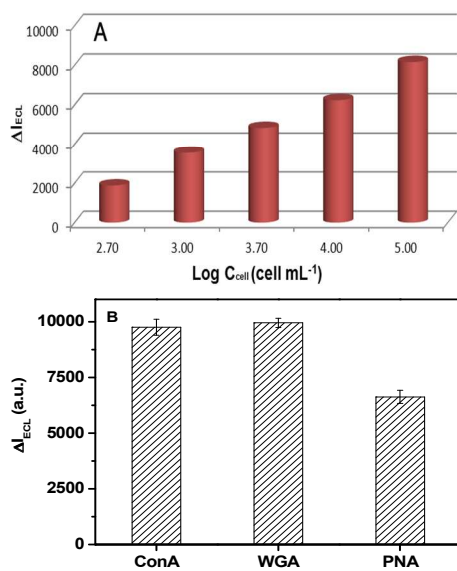
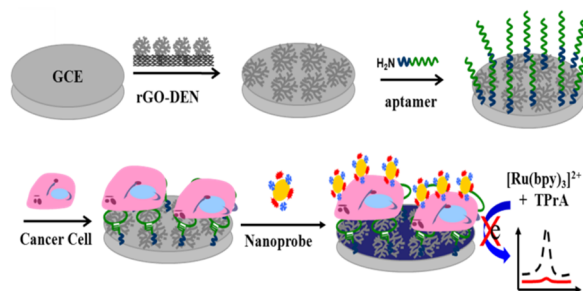


Table of Contents



Multivalent recognition and enzyme-responsive aptamer electrogenerated chemiluminescence biosensor for the analysis of cancer cell and its surface glycan expression.